J Biomol NMR (2014) 59:1–14
DOI 10.1007/s10858-014-9822-6

PERSPECTIVE

Dynamics in the solid-state: perspectives for the investigation of amyloid aggregates, membrane proteins and soluble protein complexes

Rasmus Linser · Riddhiman Sarkar · Alexey Krushelnitzky · Andi Mainz · Bernd Reif

Received: 19 December 2013 / Accepted: 26 February 2014 / Published online: 5 March 2014

Abstract Aggregates formed by amyloidogenic peptides and proteins and reconstituted membrane protein preparations differ significantly in terms of the spectral quality that they display in solid-state NMR experiments. Structural heterogeneity and dynamics can both in principle account for that observation. This perspectives article aims to point out challenges and limitations, but also potential opportunities in the investigation of these systems.

Keywords MAS solid-state NMR · Protein dynamics · Amyloid fibrils · Membrane proteins · Soluble protein complexes

Introduction

The NMR spectral quality for amyloid and membrane protein preparations in the solid-state differs significantly between different systems. Aggregates formed by the Alzheimer's disease Aβ peptide and the *E. coli* multi drug resistance transporter EmrE yield relatively broad resonances (Tycko 2006; Agarwal et al. 2007), whereas others like fibrils formed by the prion protein HET-s and the membrane protein bacteriorhodopsin display very favorable spectral properties (Wasmer et al. 2008; Linser et al. 2011). Obviously, structural heterogeneity can yield inhomogeneous broadening which results in a reduced spectral dispersion. On the other hand, dynamics can have a major impact on the apparent resolution. Structural heterogeneity and dynamics are linked by the activation barrier of a dynamic process. In fact, interconversion of fibril polymorph structures on a timescale of several weeks was shown recently by Tycko and co-workers (Qiang et al. 2013). Macroscopically, these dynamic processes are reflected in chemical exchange between an amyloid fibril-type conformation and a soluble molecule (Carulla et al. 2005; Narayanan et al. 2005; Fawzi et al. 2011). In solution, this exchange process occurs on a timescale of seconds to days. These observations raise the question about the fundamental processes at the atomic level which results in dissociation of a single peptide from the amyloid fibril. Mechanical stress or sonification results in fibril fragmentation. This process generates open ends at which polymerization and de-polymerization can occur. In order to dissociate a single peptide, many hydrogen bonds need to be broken simultaneously. For this to happen, a concerted motion is required. So far, the mechanisms at the atomic level which result in dissociation of aggregated peptides are not very well understood.

For soluble, globular proteins, the protein folding funnel is typically very steep. According to Anfisen's dogma, for a given amino acid sequence only one minimum is populated (Anfinsen 1973). On the other hand, for insoluble

R. Linser
Department of Biological Chemistry and Molecular Pharmacology, Harvard Medical School, 240 Longwood Ave, Boston, MA 02115, USA

R. Sarkar · A. Mainz · B. Reif (✉)
Department of Chemie, Munich Center for Integrated Protein Science (CIPSM), Technische Universität München (TUM), Lichtenbergstr. 4, 85747 Garching, Germany
e-mail: reif@tum.de

R. Sarkar · A. Mainz · B. Reif
Deutsches Forschungszentrum für Gesundheit und Umwelt (HMGU), Helmholtz-Zentrum München, Ingolstädter Landstr. 1, 85764 Neuherberg, Germany

A. Krushelnitzky
Institut für Physik – NMR, Martin-Luther-Universität Halle-Wittenberg, Betty-Heimann-Str. 7, 06120 Halle (Saale), Germany

proteins—in particular for amyloid fibrils—it is generally assumed that this dogma does not hold true, and that amyloids can adopt different conformations, a phenomenon which is referred to as fibril polymorphism. For amyloid fibrils, and maybe for solid-state samples in general, the energy landscape for the "fold" of a particular conformer appears to be characterized by a less distinct profile with more subtle differences between isolated local minima and higher activation barriers. This seems to be a consequence of steric hindrance and higher activation barriers for molecular reorientation due to molecular crowding.

Enzymatic turnover or recognition of ligands is directly coupled to dynamics (Williams et al. 1995; Cole et al. 2002; Henzler-Wildman et al. 2007a, b; Lange et al. 2008). Even though different kinds of functionality rely on dynamics on very different amplitudes and timescales, the critical motility involved in protein functionality seems to occur on a μs timescale. For solid-state preparations, the characteristic time seems to be larger due to the higher molecular weight of the complexes or the anchoring within the lipid matrix. The catalytic rate of rhodopsin in vivo is on the order of 600–1,300 s^{-1} (Heck et al. 2001). ATP synthase is thought to revolve at 650 revolutions per second (Ueno et al. 2005). Similarly, the glucose transporter works with a rate on the order to 300 s^{-1} (Gennis 1989; Stein 1990).

Motion on different timescales can induce deleterious effects on spectral quality: μs-ms time scale motion leads to exchange broadening. ns–μs timescale dynamic processes yield N–H^{α} and N–H^{β} differential relaxation. Standard ^{1}H decoupled solid-state NMR experiments which average H^{α}/H^{β} proton spin states would yield compromised resolution under these circumstances. Solid-state NMR spectroscopy holds a great potential for the study of dynamic processes, as relaxation results from local structural fluctuations only, and is not affected by overall tumbling. This perspectives article aims to highlight how protein dynamics influence the resolution of MAS solid-state NMR resonance line shapes. The hypotheses and speculations made are supplemented with experimental data for a microcrystalline sample of the chicken α-spectrin SH3 domain, the β-barrel membrane protein OmpG, fibrils of the Alzheimer disease β-amyloid peptide, and different assemblies of the 20S proteasome of *Thermoplasma acidophilum*.

Microcrystalline proteins

The highest structural order is expected for a microcrystalline protein preparation. Nevertheless, many residues in the sequence of the α-spectrin SH3 domain show a significant amount of dynamics. Figure 1a represents a selected region of a ^{1}H,^{15}N correlation experiment recorded for a perdeuterated micro-crystalline sample of the α-spectrin SH3 domain, in which exchangeable deuterons are in part back-substituted with protons. Scalar coupling based INEPT experiments (red) and dipolar coupling based CP experiments (black) are superimposed. The N-terminus (e.g., residues T4, G5) is highly flexible and suppressed in the experiments using cross polarization. On the other hand, the resonances of residues located in the N-Src loop (e.g. T37) are exchange broadened and can be observed only in the CP version of the experiment. Typical values for ^{1}H and ^{15}N T_2 relaxation times for the α-spectrin SH3 domain, as well as the experimental line widths are summarized in Table 1.

In the past, we quantified the dynamics of the SH3 domain in the framework of an extended model-free formalism (Chevelkov et al. 2009b). Other groups have worked on the dynamic characterization of ubiquitin (Schanda et al. 2010), superoxide dismutase (Knight et al. 2012) and thioredoxin (Yang et al. 2009). For a quantitative description of motion on two timescales (amplitude and correlation times), at least four linear independent observables are required. We used a combination of ^{15}N–R_1 relaxation rates measured at different field (Chevelkov et al. 2008), ^{1}H–^{15}N dipole–dipole, ^{15}N CSA cross-correlated relaxation, which allows to quantify $J(0)$ spectral density functions related to T_2 type relaxation rates (Chevelkov et al. 2007a, b), as well as dipolar order parameters obtained from CPPI measurements (Chevelkov et al. 2009a). Alternatively, site-specific incoherent T_2 type relaxation rates can be obtained from $T_{1\rho}$ measurements (Akasaka et al. 1983). This approach has been implemented recently for GB1 (Lewandowski et al. 2011b), ubiquitin (Tollinger et al. 2012), and the α-spectrin SH3 domain (Krushelnitsky et al. 2010; Zinkevich et al. 2013).

So far, only model-free motional analyses has been carried out. Obviously, the long-term goal should be to obtain model dependent information on dynamics. The quantification of the asymmetry parameter η of ^{2}H tensors (Hologne et al. 2005, 2006) or of dipolar coupling (Schanda et al. 2011) allows to get information on motional models, such as jump angle and population of side chain rotameric states. Additional information might come from selectively side chain protonated samples in an otherwise deuterated matrix (Asami et al. 2010; Asami and Reif 2013). Availability of an X-ray structure facilitates the analysis of the dynamic behaviour of the protein, since the structure can be employed as a starting point for a molecular dynamics trajectory (Chevelkov et al. 2007c, 2010; Mollica et al. 2012). Such a trajectory is of tremendous help in the interpretation of the NMR data. With the availability of more experimental data, e.g. from RAP labeled samples (Asami et al. 2010), the high degeneracy of data should enable a model-dependent analysis of motion without the need for a MD trajectory.

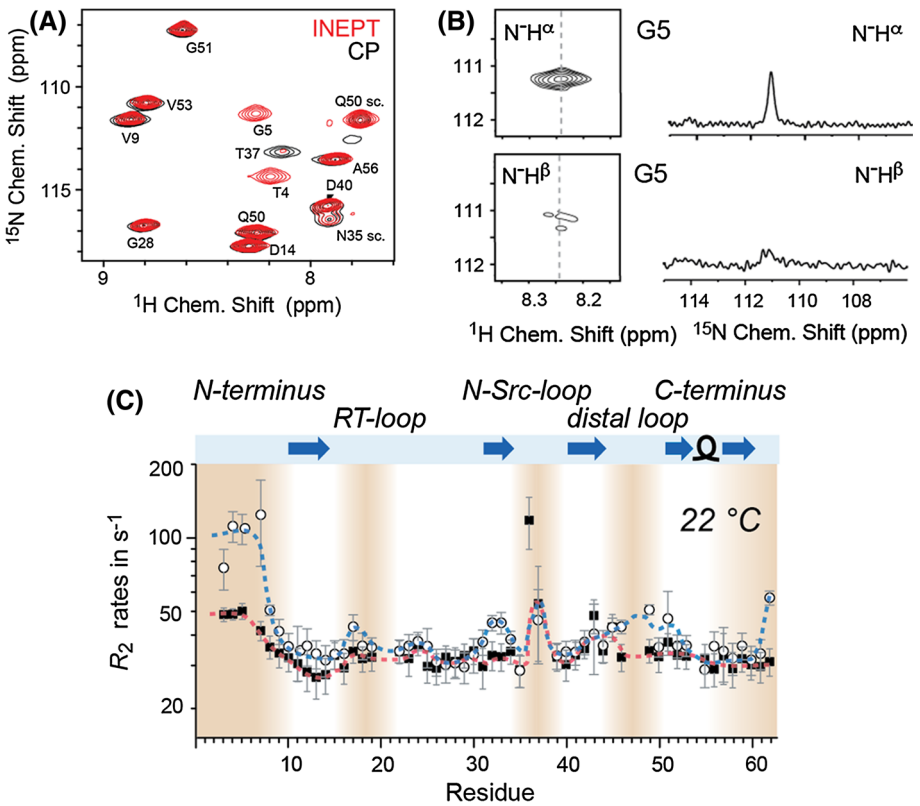

Fig. 1 α-spectrin SH3 $^{1}H,^{15}N$ correlation spectra and relaxation data. **a** Experiments employing scalar (*red*) and dipolar magnetization transfers (*black*) are superimposed. The experiments were recorded on a spectrometer operating at a ^{1}H Larmor frequency of 600 MHz, and at a temperature of 22 °C. The MAS frequency was set to 24 kHz. **b** $N^{-}H^{\alpha}$ and $N^{-}H^{\beta}$ spin-state selective experiments showing the spectral region containing G5. A substantial difference in intensity for the coherences $N^{-}H^{\alpha}$ and $N^{-}H^{\beta}$ are observed, indicating dynamics in the ns–μs regime. Separation of spin-states is achieved by employing the spin-state selective pulse schemes (Linser et al. 2010). **c** Relaxation rates for coherences $N^{-}H^{\alpha}$ (*black squares*) and $N^{-}H^{\beta}$ (*white circles*). Differential relaxation is indicative for large amplitude ns–μs dynamics (Chevelkov et al. 2007a; Skrynnikov 2007). *Dashed lines* are drawn in order to guide the eye. Large differential relaxation rates are found for D62, the N-terminus and the distal loop involving residues 45–50

Table 1 ^{1}H and ^{15}N T_2 relaxation times, theoretical and experimental line widths for a microcrystalline sample of perdeuterated α-spectrin SH3, recrystallized from a buffer containing 75 % D_2O

	$^{1}H^{N}$ T_2 [ms]	^{1}H LW (calc) [Hz]	^{1}H LW (exp) [Hz]	^{15}N T_2 [ms]	^{15}N LW (calc) [Hz]	^{15}N LW (exp) [Hz]
α-spectrin SH3	12.4 ± 0.9	25.7 ± 1.8	25 ± 5	21.8 ± 3.3	14.6 ± 2.2	15 ± 3

T_2 was measured in an echo experiment with one 180° pulse in the center of the incremented delay for the H^{N} bulk signal. The experiments were recorded at a magnetic field strength of 14.1 T and a MAS rotation frequency of 20 kHz and setting the effective temperature to 25 °C

Interestingly, the quantitative dynamic analysis of site-resolved mobility in the α-spectrin SH3 domain shows that the N-terminus is flexible on a high ns timescale (Fig. 1b). We observed temperature dependent transverse relaxation rates for $N–H^{\alpha}$ and $N–H^{\beta}$ differing by up to a factor of 4 for the same amide. Consequently, application of TROSY-type experiments significantly improves the spectral quality of this part of the protein (Linser et al. 2010). This effect is due to substantial cross-correlated relaxation between dipolar and CSA-related relaxation mechanisms (differential relaxation), as shown in Fig. 1c. Use of this effect allows to improve the relaxation properties of the involved nuclei in regions of the protein undergoing high ns timescale motion.

Limits of resolution

In the solid-state, inhomogeneous and homogeneous mechanisms contribute to the NMR line width. Inhomogeneous broadening results in chemical shift dispersion, whereas homogeneous broadening is a consequence of relaxation processes. Obvious factors such as the accuracy of the magic angle, the decoupling performance and the quality of the shim contribute to resonance line width. In

deuterated samples, the spectral quality cannot be improved any further at a certain level of deuteration (Chevelkov et al. 2006; Zhou et al. 2007a, b; Akbey et al. 2010; Lewandowski et al. 2011a), indicating that dipolar interactions are not limiting spectral resolution. Similarly, spinning angle mis-adjustment results in an increase of the line width by a few Hertz (Chevelkov et al. 2007b; Agarwal et al. 2009). The shim contributes less than 1 Hz to proton line width. Back-calculation of the line width from the NMR relaxation data (Chevelkov et al. 2009b) yields a dynamic contribution due to local motion which is on the order of less than 1 Hertz for the majority of all amides (Fig. 1c, the difference rate is proportional to the local correlation time of the motion).

A property which is more difficult to control is the Anisotropic Bulk Magnetic Susceptibility (ABMS) (Alla et al. 1980; Vanderhart et al. 1981; Samoson et al. 2001). ABMS produces a dispersion of chemical shifts, similar to ring current shifts, and is a result of the amorphous arrangement of protein microcrystals in the NMR rotor, potentially interrupted with water and void volume. ABMS cannot be suppressed simply by magic angle spinning. However, since the Hamiltonian for the ABMS interaction has a similar dependence as the isotropic chemical shifts on the nuclear spin part (Samoson et al. 2001), application of a CPMG pulse train can induce significant line narrowing (Garroway 1977; Cowans et al. 1993; Wiench et al. 2008). The spin-echo FID yields a spike spectrum upon Fourier transformation, in which the distance between two spikes is determined by the CPMG frequency. The isotropic chemical shift information can be reconstructed from the spike-spectrum, provided the CPMG frequency is smaller than the frequency difference between two chemical shifts (Cowans et al. 1993). Analogous methods have been found useful applications to enhance sensitivity for ^{29}Si (Wiench et al. 2008; Bocan et al. 2012). However for crowded spectra, it is difficult to implement a CPMG train where the aforementioned condition is satisfied. As an example, Fig. 2a shows that the ^{15}N line width in a deuterated, micro-crystalline sample of the α-spectrin SH3 domain can be reduced from 10 Hz to approximately 6 Hz upon application of a CPMG pulse train. Even though relatively small in absolute numbers, ABMS is thus a major contributor to the residual line width in these samples. A 2D ^{1}H detected ^{15}N/^{1}H correlation experiment (Fig. 2b) was recorded with (black) and without (red) application of CPMG during detection. Due to the cancellation of the ABMS during the CPMG train, the FID lasts much longer and an extended acquisition time was employed ($t^{aq}_{CPMG} = 147$ ms, $t^{aq}_{ref} = 50$ ms). It remains to be seen if and how the isotropic chemical shift information can be extracted from such a spectrum, in cases where the CPMG frequency is higher than the smallest chemical shift differences. We note that CPMG experiments can in principle yield information on chemical exchange processes, and thus on μs–ms dynamics (Lewandowski et al. 2011b; Tollinger et al. 2012). Some care has to be taken to differentiate between chemical exchange processes and refocussing of ABMS.

Amyloid aggregates

In contrast to crystalline proteins, amyloids might be considered as one-dimensional crystals. In that sense, a somewhat lower resolution is expected for amyloids in comparison to microcrystalline samples. For amyloids, however, structural heterogeneity might have a major impact on the experimental spectral properties. For a globular protein, the structure is defined by the amino acid sequence in a unique way (Anfinsen 1973). It is assumed that the same dogma does not apply not amyloids and that amyloid fibrils are not a native fold. Misfolding is rather determined by the chemical properties of the amide backbone (Fandrich et al. 2001). As a consequence, a certain degree of polymorphism is expected in the structure of an amyloid fibril (Petkova et al. 2006; Paravastu et al. 2008). On the other hand, functional amyloids have been discovered to be important elements in bacterial and fungal biofilm formation (Chapman et al. 2002). Fungal prions have been shown to be involved in prion replication (Maddelein et al. 2002). Functional amyloids also play a role in mammalian skin pigmentation (Fowler et al. 2006), and as storage depot for hormones (Maji et al. 2009). This has raised the question whether amyloid fibrils can be considered a functional fold. Riek and Greenwald suggested that an amyloid might even have been the first fold in the early stages of life on earth (Greenwald and Riek 2012). In fact, amino acid sequences that are commonly found in amyloidogenic peptides and proteins occur as well in complex biomolecular machines, such as the nuclear pore complex (Halfmann et al. 2012; Labokha et al. 2013), and are part of the low complexity sequences in RNA binding proteins (Kato et al. 2012; Kim et al. 2013). The fact that an amyloid aggregate can have a function would imply a low structural heterogeneity (at least in certain parts of the protein sequence), and thus a high NMR spectral quality. For the Alzheimer's disease Aβ peptide, which is a key mediator of Alzheimer's disease pathology, such a function in the aggregated state has not been reported yet. Aβ is often thought to be an incidental catabolic by-product that lacks a normal physiological role. However, Aβ has been shown to be a specific ligand for a number of different receptors (Le et al. 2001), transported by complex trafficking pathways (Tanzi et al. 2004), and able to induce pro-inflammatory activities (Halle et al. 2008). Furthermore, Aβ was shown to play a role in activity-dependent regulation of synaptic vesicle release

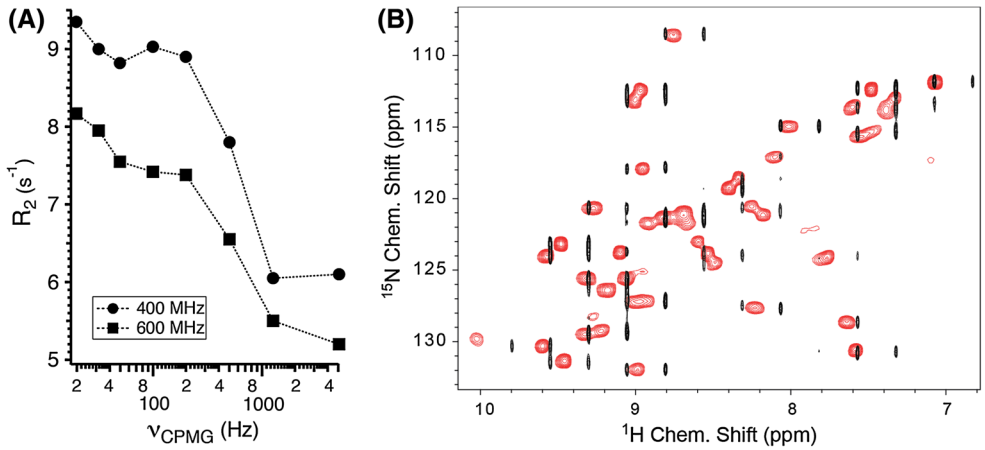

Fig. 2 **a** ^{15}N R_2 relaxation rate upon application of a CPMG pulse train for the bulk amid resonances in α-spectrin SH3. ν_{CPMG} is defined as $1/(\tau - 180 - \tau)$. The decay in the relaxation rates is due to the refocussing of ABMS. **b** N/H correlation with a CPMG pulse train applied during acquisition (*black*), superimposed with a regular N/H correlation (*red*) for α-spectrin SH3. In the CPMG experiment, $\tau = 5$ ms was employed. The acquisition time was set to 147 ms, whereas the signal was acquired for only 50 ms in the N/H reference experiment. Both spectra were recorded at a spectrometer operating at 400 MHz. In the CPMG experiment, resonances appear significantly more narrow. However, application of the CPMG refocussing pulses results in undefined isotropic shifts

(Abramov et al. 2009), and suggested to have antimicrobial activity (Soscia et al. 2010).

Amyloid assemblies have been reported to be dynamic assemblies. Dobson and co-workers demonstrated that SH3 molecules constantly dissociate from and re-associate with PI(3)K-SH3 fibrils (Carulla et al. 2005). ESI–MS H/D exchange studies yielded two distinct populations for the fibrillar assembly after exposure of the fibrils to exchange, corresponding to a population of fast-exchanging and slow-exchanging molecules. Fit of the MS data to a model in which monomers can be added to the fibril ends yields a recycling time on the order of 2–20 days, depending on the length of the fibril (Carulla et al. 2005). By contrast, Clore and co-workers found faster exchange rates in case of the Alzheimer's disease peptide Aβ40 and Aβ42 (Fawzi et al. 2010, 2011). Quantitative fit of ^{15}N DEST (Dark-state Exchange Saturation Transfer) data yield dissociation rates which are on the order of $k_{off} = 50$–100 s^{-1}, depending on concentration and temperature. Exchange between an aggregated and a soluble form of the Aβ40 was also observed by STD-NMR experiments (Narayanan et al. 2005). Recently, this interconversion could be shown directly by solid-state NMR experiments (Qiang et al. 2013). Tycko and co-workers have shown that an isolated fibril polymorph structure can convert into another polymorph on a timescale of several weeks. Dynamics in a C-terminally truncated variant of the human prion protein (HuPrP23-144) has been probed in $T_{1\rho}$ type experiments (Helmus et al. 2008, 2010). It is found that the rigid core residue in the prion fibrils undergoes μs-ms timescale motion. It will be interesting to see how this dynamics compares to the exchange dynamics observed e.g. in DEST experiments.

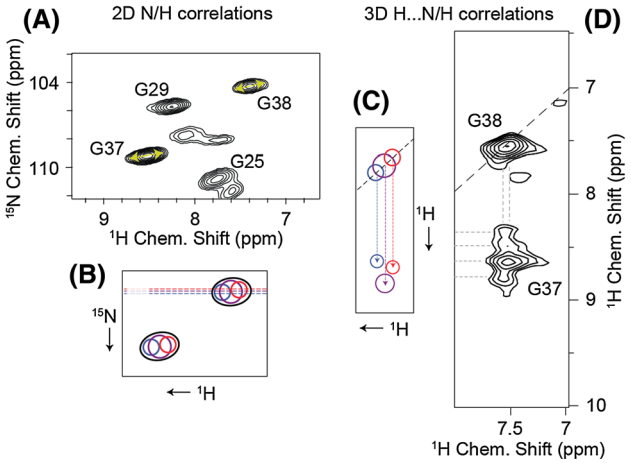

Fig. 3 MAS solid-state NMR experiments for a fibril sample of the perdeuterated Alzheimer's disease peptide $A\beta^{1-40}$. Exchangeable sites are back-substituted with 20 % protons. **a** 2D N/H-correlation spectrum (selected region) (Linser et al., 2011). **b/c** Schematic representation of a 2D N/H and 3D ^{15}N edited H/H correlation spectrum using RFDR for homonuclear mixing. The different colors indicate three different fibril conformers. **d** Experimental ^{15}N edited H/H correlation spectrum focussing on the cross peak between the amide protons of residues G37 and G38 in $A\beta^{1-40}$

The broad proton lines observed previously in proton detected experiments (Fig. 3) recorded for fibrils of per-deuterated Alzheimer's disease Aβ40 (Linser et al. 2011; Agarwal et al. 2013) raise the question about the origin of line width in these kind of samples. For fibrils of α-synuclein fibrils (Zhou et al. 2012) and hydrophobins (Morris et al. 2012), which are functional amyloids affecting surface properties of fungal spores, a similar spectral quality is obtained. These common observations might indicate that

Table 2 ^{1}H, ^{15}N T_2 relaxation times, theoretical and experimental line widths for a fibril sample of perdeuterated Aβ^{1-40}

	$^{1}H^{N}$ T_2 [ms]	^{1}H LW (calc) [Hz]	^{1}H LW (exp) [Hz]	^{15}N T_2 [ms]	^{15}N LW (calc) [Hz]	^{15}N LW (exp) [Hz]
Aβ^{1-40}	8.2 ± 0.2	38.8 ± 1.0	170 ± 47	13.5 ± 0.2	23.6 ± 0.3	38 ± 10

All experimental parameters as magnetic field strength, MAS rotation frequency and temperature were the same as described above for the microcrystalline SH3 sample

the observed broad amide resonances could be a general phenomenon.

Interestingly, heteronuclear detected experiments of a protonated fibril sample (Lopez del Amo et al. 2012a, b) display a reasonable resolution which seems to be limited by evolution of scalar couplings (ca. 100–130 Hz in the ^{13}C dimension, 38 ± 10 Hz for ^{15}N). For preparation of protonated and deuterated fibrils samples, the same seeds have been employed. In the deuterated fibril preparation, the line width of protons is significantly larger in comparison to the line width of nitrogens (170 ± 47 Hz for ^{1}H, and 38 ± 10 Hz for ^{15}N, Table 2). This is surprising as the effective spectral frequency range (in Hz) for the proton and nitrogen dimension is comparable (3 vs. 30 ppm). Therefore, a similar sensitivity with respect to conformational changes would be expected for both nuclei. For protons, however, a fourfold reduced resolution is observed.

Comparison of the ^{1}H line width and the T_2 decay time measured in a spin-echo experiment (Table 2) shows that the proton resonance lines are inhomogeneously broadened, which is presumably due to a superposition of resonances from multiple fibril polymorphs. Similarly, the skew, asymmetric peak shapes in Fig. 3a seem to indicate superposition of multiple resonances reflecting a certain degree of conformational heterogeneity. Higher dimensional experiments might allow to resolve contributions from different polymorphs. A schematic representation of the expected signal pattern is shown in Fig. 3c. In fact, multiple cross peaks are observed for the correlation H^{N}(G38)–H^{N}(G37) in an ^{15}N-edited homonuclear H/H NOESY-type experiment (Fig. 3d). In the future, experiments of that kind might allow a site-specific characterization of conformational heterogeneity in an amyloid fibril.

In order to find out whether line broadening originates from ns–μs timescale motion, we recorded TROSY-type experiments in the solid-state (Fig. 4). Similar as above for the micro-crystalline preparation of the α-spectrin SH3 domain (Fig. 1b), differential broadening of the ^{15}N–H^{α} (red) and ^{15}N–H^{β} spin-states would be expected, in case motionally induced relaxation contributes significantly to the resonance line width. However, no significant differences for the intensities of the two spin states are observed, indicating that no large amplitude ns-μs timescale motion occurs. Increase of the exchange dynamics would potentially result in more narrow resonance lines.

The variation of ^{1}H and ^{15}N shifts seem to be concerted yielding to oval-shaped, tilted peaks (Fig. 3a). The tilt is very similar for most peaks with a characteristic slope of roughly 13 ± 0.7 (Hz,^{1}H)/(Hz,^{15}N). The effect of pressure might explain the observed N/H peak shapes in part. It is known that pressure has a significant impact on NMR chemical shifts, in particular for exchangeable protons (Arnold et al. 2002; Kitahara et al. 2013).

The pressure acting on a sample in a volume element at a distance r_0 from the rotor axis can be approximated by Pascal's law (Fig. 5). r_0 refers to the inner radius of the MAS rotor, ρ describes the density of the protein and ν_R represents the MAS rotation frequency. The protein density can be assumed to be 1.4 g/cm^{-3} (Quillin et al. 2000). According to this formula, the maximum pressure for a rotating sample in a 3.2 mm MAS rotor (r_0 = 1.2 mm, ν_R = 20 kHz) is on the order of 320 bar (32 MPa). It was found that the pressure induced proton chemical shift change is in the range of 0.4 ppm GPa^{-1} (Arnold et al. 2002). This yields a theoretical proton chemical shift distribution of about 10 Hz for a spectrometer operating at 14.1 T (600 MHz), assuming a homogeneous distribution of the sample in the rotor. In reality, the pressure gradient is presumably smaller, as the sample sediments on the walls of the rotor, with not much protein being localized close to the rotor axis. Pressure induced ^{15}N chemical shift changes $\Delta\delta_P$ are on the order of 1.5–2.5 ppm GPa^{-1}. Interestingly, reduced local compressibilities are observed for β-sheets with $\Delta\delta_{P,N}$ = 1.5 ppm GPa^{-1} (Akasaka et al. 1999). For ^{15}N, therefore a distribution of resonances within 3 Hz would be expected. Overall, the expected differences appear to be rather small, and it seems that pressure does not contribute significantly to the experimental (proton) line width. In addition to chemical shift changes from isotropic compression, pressure induced mechanical deformations of the investigated sample could be responsible for the observed resonance line broadening. Due to their shape, amyloid fibrils appear to be more prone to deformation in comparison to microcrystalline protein preparations. This might be another factor, which might result in larger broadenings for amyloid fibrils in comparison to crystalline samples.

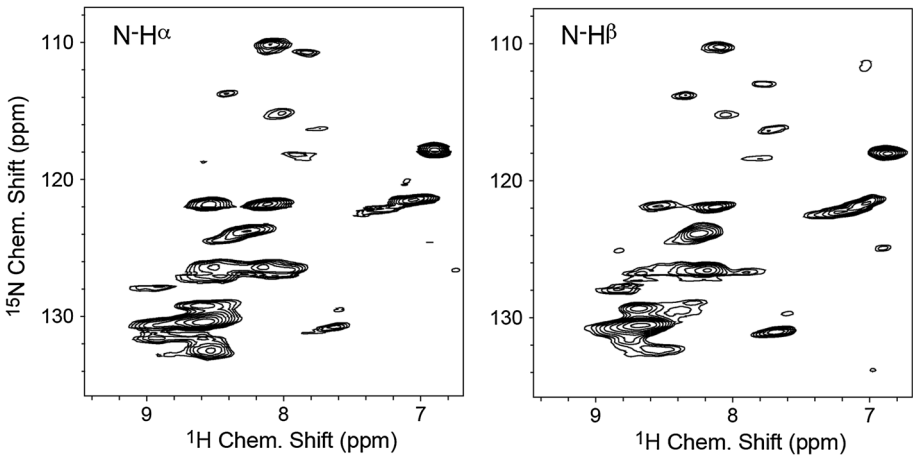

Fig. 4 Comparison of 2D N/H correlation spectra selecting the $^{15}N^{-}H^{\alpha}$ (*left*) and $^{15}N^{-}H^{\beta}$ (*right*) spin-states in a deuterated Aβ(1-40) fibril sample. No significant differences are observed, indicating that no large amplitude ns–μs timescale motion occurs (Linser et al. 2010). The experiments were recorded at 900 MHz within 3 h, employing $t_1^{max} = 30$ ms. The MAS rotation frequency was adjusted to 20 kHz. The effective sample temperature was set to 20 °C

$$p(r) = \int_0^{r_0} dr\ \rho\ a(r) = \rho \int_0^{r_0} dr 4\pi^2 \nu_R^2\ r$$
$$= 2\pi^2 \nu_R^2\ \rho\ r_0^2$$

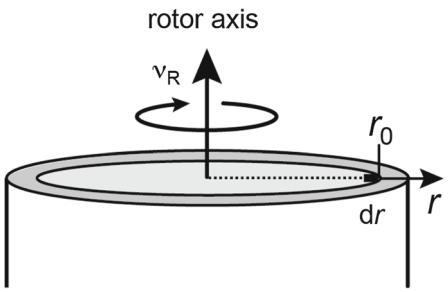

Fig. 5 Pressure acting on a rotating sample under magic angle spinning

Taken together, the line width in our Aβ40 fibril preparations is determined by structural heterogeneity and/or by dynamics on a μs–ms timescale. Measurements carried out at increased temperature in principle would allow one to get into the fast-exchange limit. Currently, the experimentally available temperature range is limited as sealing of NMR rotors is difficult to prevent solvent evaporation and dehydration over time.

Membrane proteins

Using solid-state NMR methodology, the first structures of membrane proteins containing multiple membrane spanning helices have been determined using solid-state NMR methodology (Park et al. 2012; Shahid et al. 2012; Wang et al. 2013a). In these cases, the resolution in $^{13}C/^{13}C$ and $^{13}C/^{15}N$ correlation experiments is excellent. Other systems display a much less favorable spectral dispersion (Agarwal et al., 2007). In addition to the crystallization process itself, Reconstitution of a membrane protein into the correct lipid environment is obviously an issue, and use of the *wrong* lipids might result in heterogeneity or exchange broadening. Collection of cell wall fragments which contain the over-expressed membrane protein, that are packed directly into a MAS rotor without any further purification and reconstitution might be a solution to that issue (Renault et al. 2011; Jacso et al. 2012; Takahashi et al. 2013; Wang et al. 2013b). This approach, however, suffers typically from low sensitivity. Dynamic Nuclear Polarization (DNP) is needed to regain the sensitivity necessary to acquire multidimensional NMR experiments (Hall et al. 1997). At least for certain samples, the decrease in resolution due to sample freezing can be overcome by going to higher-field instrumentation (Lopez del Amo et al. 2013). In standard solid-state NMR experiments performed at room temperature, sample heating due to high-power RF irradiation during proton acquisition can compromise sample integrity (Linser et al. 2007).

For a long time, crystallization of G protein coupled receptors (GPCRs) was hampered due to their large intrinsic dynamics which prevented the growth of well diffracting protein crystals. Directed mutagensis (Sarkar et al. 2008; Chen et al. 2012; Schlinkmann et al. 2012),

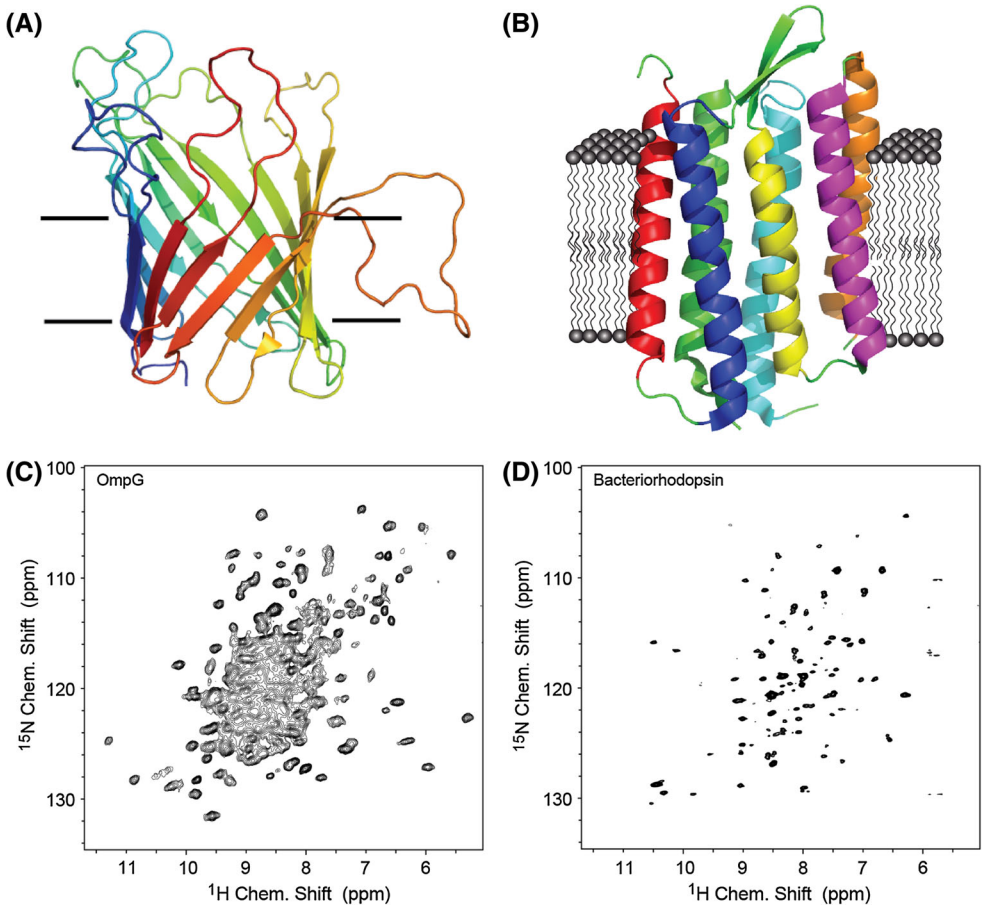

Fig. 6 Structural model of OmpG (PDB ID: 2JQY) (**a**), and Bacteriorhodopsin (bR, PDB ID: 1C3W) (**b**). The respective ^{1}H,^{15}N correlation spectra are shown in (**c**) and (**d**). bR was prepared from native purple membranes (Patzelt et al. 1997), whereas OmpG was reconstituted in *E.coli* lipid extract (Hiller et al. 2005). Figure reproduced with permission from Wiley (Linser et al. 2011)

binding of antibodies (Rasmussen et al. 2007), or GPCR engineering (Rosenbaum et al. 2007) was needed to suppress this motional flexibility. In fact, membrane proteins are not tightly packed, but contain a considerable number of internal cavities that differ in volume, polarity and solvent accessibility as well as in their filling with internal water (Rose et al. 2013). These cavities are supposed to be regions of high physical compressibility. In that sense, a large degree of conformational flexibility is expected and needed to facilitate transitions between different functional states.

In comparison to ^{13}C or ^{15}N, protons seem to be a more sensitive probes to detect either structural heterogeneity and/or dynamics. Figure 6 shows 2D N/H correlation spectra of OmpG and bacteriorhodopsin (bR) (Linser et al. 2011). For both preparations, the labeling pattern as described above for the α-spectrin SH3 domain has been employed (perdeuterated at non-exchangeable sites, and 10–30 % protonation at exchangeable positions). Acquisition and processing parameters are comparable for the experiments described here and above. Obviously, the spectral quality for these two preparations is very different. Values for the ^{1}H and ^{15}N T_2 decay time from spin-echo experiments, as well as the calculated and experimental line width are summarized in Table 3. Other deuterated protein preparations in the solid-state such as the 20 kDa membrane protein DsbB reconstituted in *E. coli* lipids (Zhou et al. 2012) and the DMPC/DMPA reconstituted proteorhodopsin (Ward et al. 2011) yield a ^{1}H,^{15}N spectral resolution which is comparable to the OmpG preparation.

For OmpG, signal intensities for dipolar-transfer based experiments drastically increase at lower temperatures (3 °C). However, also at room temperature dipolar transfers are possible. This is in contrast to the observed broadening of resonances in the flexible N- and C-terminus in the SH3 domain of α-spectrin, for which only scalar transfers give rise to detectable signal. This indicates that the amplitude of motion in OmpG must be much smaller. Comparing TROSY/anti-TROSY 2D N/H experiments (without and with additional relaxation delays to enhance differences) does not indicate a large amount of differential relaxation (data not shown), suggesting that ns-µs

Table 3 ^{1}H, ^{15}N T_2 relaxation times, theoretical and experimental line widths for perdeuterated samples of the outer membrane β-barrel protein OmpG and bacteriorhodopsin (bR)

	$^{1}H^{N}$ T_2 [ms]	^{1}H LW (calc) [Hz]	^{1}H LW (exp) [Hz]	^{15}N T_2 [ms]	^{15}N LW (calc) [Hz]	^{15}N LW (exp) [Hz]
OmpG in						
Protonated lipids	6.8 ± 0.5	46.8 ± 3.4	121 ± 42	10.0 ± 1.0	31.8 ± 3.2	60 ± 34
Deuterated lipids	9.2 ± 1.0	34.6 ± 3.8	101 ± 31	11.1 ± 2.3	28.7 ± 6.2	53 ± 23
Bacteriorhodopsin (bR)	n.d.	–	27 ± 7	n.d.	–	11 ± 3

All experimental parameters were the same as described above for the microcrystalline SH3 sample

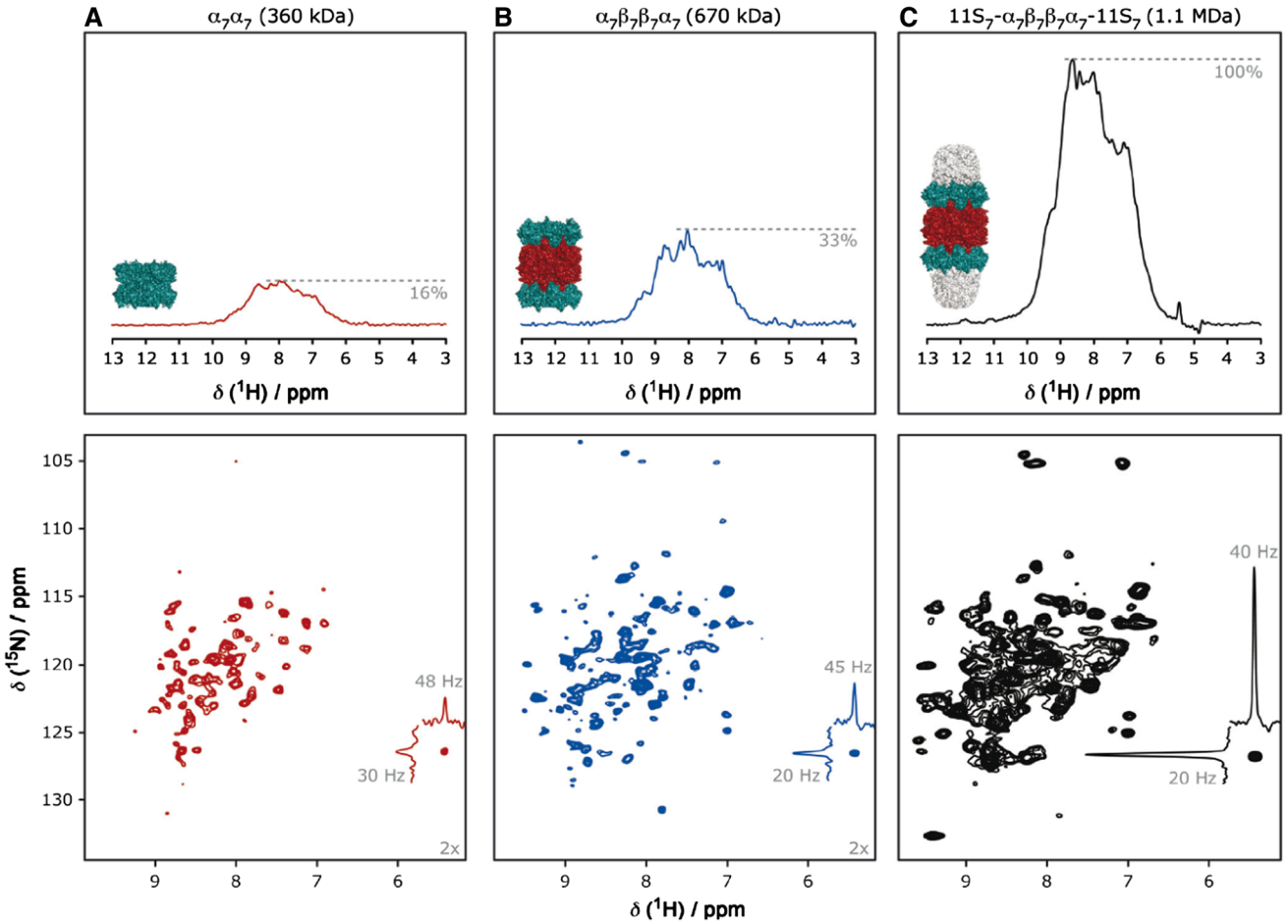

Fig. 7 Proton-detected MAS experiments and the effect of increasing molecular weight for different assemblies of the 20S proteasome of *Thermoplasma acidophilum*. Cross polarization (CP) based 2D ^{1}H-^{15}N correlation spectra are shown on the bottom, the corresponding 1D versions are represented on the top for the 360 kDa $\alpha_7\alpha_7$ (**a**), the 670 kDa $\alpha_7\beta_7\beta_7\alpha_7$ (**b**) and the 1.1 MDa 11S-$\alpha_7\beta_7\beta_7\alpha_7$-11S complex (**c**). The spectra were recorded at 0 °C and with 22 kHz MAS. Acquisition and processing parameters were identical. The signal intensities of ^{15}N-filtered ^{1}H-1D spectra are normalized to account for the different concentrations of the α-subunit. The calculated fraction of sedimented protein amounts to 97.7, 98.8 and 99.7 % for $\alpha_7\alpha_7$, $\alpha_7\beta_7\beta_7\alpha_7$ and 11S-$\alpha_7\beta_7\beta_7\alpha_7$-11S, respectively. Figure reproduced with permission from Wiley (Mainz et al. 2013)

dynamics do not significantly influence resonance line width for OmpG. On the other hand, membrane proteins undergo μs timescale rotational diffusion within the lipid bilayer (Saffman et al. 1975; Austin et al. 1979; Cherry 1979, 2005). This motion is as well detected in solid-state NMR experiments (Park et al. 2006). For the transmembrane helix of the channel-forming domain of the protein Vpu from HIV-1 in in DOPC/DOPG bilayers, a characteristic rotational diffusion time on the order of 10 μs was found. In aligned phospholipid bilayers, this motion is exploited to yield better resolved PISEMA spectra (Lu et al. 2012). In non-aligned, amorphous

samples the uniaxial rotation of membrane proteins is employed to determine the relative orientation of a membrane helix with respect to the phospholipid bilayer (Hong et al. 2006; Cady et al. 2007). On the other hand, local motion in sensory rhodopsin was shown to occur on a μs timescale (Good et al. 2014). It will be interesting to see how these two types of motion can possibly be separated.

The resolution in DMPC/DMPA reconstituted proteorhodopsin (Ward et al. 2011) is lower in comparison to bR in native purple membranes (Linser et al. 2011). bR is found to be a trimer in the lipid bilayer (Luecke et al. 1999; Sapra et al. 2006). It thus seems that protein–protein interactions inbetween bR molecules stabilize the membrane structure and prevent rotational diffusion. DOPC reconstituted proteorhodopsin shows a hexameric arrangement of proteorhodopsin molecules (Klyszejko et al. 2008). It is thus conceivable that interdigitation of protomers from different oligomers can affect rotational diffusion in the lipid bilayer. Ladizhansky and co-worker employed DMPC/DMPA to reconstitute proteorhodopsin (Ward et al. 2011). Choice of lipids and crystallization conditions will have an effect on the architecture of the oligomeric state of proteorhodopsin, and it remains to be seen what the exact reason for the observed differences in spectral quality is.

Soluble protein complexes

In magic-angle spinning (MAS) solid-state NMR, immobilized samples are spun rapidly in a cylindrical rotor, which is inclined at an angle Θ_{MA} of 54.74° relative to the magnetic field of the NMR spectrometer (Andrew et al. 1958). Line narrowing by MAS is achieved if the correlation time of the investigated molecules is much larger than the rotor period. This is obviously the case for an immobilized solid sample. However, this also holds true for a solution of a high molecular weight protein at low temperature and high viscosity (Mainz et al. 2009, 2012). Bertini et al. have suggested that strong centrifugal forces during MAS lead to reversible protein sedimentation (Bertini et al. 2011) which effectively induces immobilization of the protein. In fact, the tumbling correlation times of protein complexes such as αB-crystallin with a molecular weight of ca. 600 kDa amount only to a few μs in the absence of MAS (Ravera et al. 2013). It might be argued that biological solid-state samples such as fibrils or membrane proteins are always prepared by sedimentation (Gardiennet et al. 2012). Nevertheless, it is remarkable that this approach allows to overcome the molecular weight limit imposed by tumbling in classical solution-state NMR. Mega-Dalton protein complexes are now accessible which previously could only be investigated in selectively methyl labeled samples in solution-state NMR (Mainz et al. 2013).

Figure 7 shows ^{15}N filtered 1D spectra acquired for different 20S proteasome complexes from *Thermoplasma acidophilum*. Interestingly, the intensity of the respective spectra increases by more than a factor of 7 when the molecular weight of the complex is increased from 360 kDa to 1.1 MDa. This is unexpected, as the calculated fraction of sedimented protein amounts to 97.7, 98.8 and 99.7 % for $\alpha_7\alpha_7$, $\alpha_7\beta_7\beta_7\alpha_7$ and 11S-$\alpha_7\beta_7\beta_7\alpha_7$-11S, respectively (Ferella et al. 2013), and indicates that there is still residual mobility in the sediment, which presumably induces exchange broadening.

On the other hand, this approach allows to circumvent sample preparation issues. Selection of the right precipitation conditions is not anymore necessary. For ligand binding studies, crystallization with and without ligand can yield different crystal forms that result in different spectral patterns. This complicates the analysis of chemical shift perturbations. In particular for weakly interacting systems, such as misfolding peptides and proteins binding to molecular chaperones, this approach might be an interesting alternative to crystallization, as the two components are very much different in terms of their solubility and co-precipitates are thus difficult to obtain.

Conclusion

Taken together, we have shown how dilution of the proton spin network can facilitate MAS solid-state NMR experiments. In microcrystalline protein samples, residual line width is not determined by the efficiency of heteronuclear dipolar decoupling, but by the anisotropic bulk magnetic susceptibility (ABMS). In amyloid aggregates and membrane proteins, additional contributions to line width originate from structural heterogeneity. We have investigated the effect of pressure on amide chemical shifts. We estimate the contribution to line width by MAS induced pressure to be on the order of 10 and 3 Hz for ^{1}H and ^{15}N, respectively. The dilute proton network allows an artifact-free analysis of dynamics in the solid-state. In contrast to micro-crystalline protein preparations where many residues undergo ns–μs motion, it seems that amyloid aggregates and membrane proteins predominantly display μs–ms dynamics. It will be exciting to see in the future how all experimental observables will be integrated to yield a model-dependent analysis of motional processes. At the same time, choice of lipids, temperature and other solution conditions can affect the achievable resolution, and it remains to be seen how this can be exploited to learn more about the functioning of membrane proteins and amyloid dynamics and propagation.

Acknowledgments This work was performed in the framework of SFB-1035/Project-B07 (German Research Foundation, DFG). This research was supported by the Helmholtz-Gemeinschaft, and the DFG (Re1435). We are grateful to the Center for Integrated Protein Science Munich (CIPS-M) for financial support. RL acknowledges the Australian Research Council for financial support in terms of a Discovery Early Career Researcher Award.

References

Abramov E, Dolev I, Fogel H, Ciccotosto GD, Ruff E, Slutsky I (2009) Amyloid-beta as a positive endogenous regulator of release probability at hippocampal synapses. Nat Neurosci 12:U1120–U1567

Agarwal V, Fink U, Schuldiner S, Reif B (2007) MAS solid-state NMR studies on the multidrug transporer EmrE. BBA—Biomembranes 1768:3036–3043

Agarwal V, Faelber K, Schmieder P, Reif B (2009) High-resolution double-quantum deuterium magic angle spinning solid-state nmr spectroscopy of perdeuterated proteins. J Am Chem Soc 131:2–3

Agarwal V, Linser R, Dasari M, Fink U, Lopez del Amo J-M, Reif B (2013) Hydrogen bonding involving side chain exchangeable groups stabilizes amyloid quarternary structure. Phys Chem Chem Phys 15:12551–12557

Akasaka K, Ganapathy S, McDowell CA, Naito A (1983) Spin–spin and spin-lattice contributions to the rotating frame relaxation of C-13 in L-alanine. J Chem Phys 78:3567–3572

Akasaka K, Li H, Yamada H, Li RH, Thoresen T, Woodward CK (1999) Pressure response of protein backbone structure. Pressure-induced amide N-15 chemical shifts in BPTI. Protein Sci 8:1946–1953

Akbey Ü, Lange S, Franks TW, Linser R, Diehl A, van Rossum BJ, Reif B, Oschkinat H (2010) Optimum levels of exchangeable protons in perdeuterated proteins for proton detection in MAS solid-state NMR spectroscopy. J Biomol NMR 46:67–73

Alla M, Eckman R, Pines A (1980) Spin diffusion and spin-lattice relaxation of deuterium in rotating solids. Chem Phys Lett 71:148–151

Andrew ER, Bradbury A, Eades RG (1958) NMR spectra recorded from a crystal rotated at high speed. Nature 182:1659

Anfinsen CB (1973) Principles that govern folding of protein chains. Science 181:223–230

Arnold MR, Kremer W, Ludemann HD, Kalbitzer HR (2002) H-1-NMR parameters of common amino acid residues measured in aqueous solutions of the linear tetrapeptides Gly-Gly-X-Ala at pressures between 0.1 and 200 MPa. Biophys Chem 96:129–140

Asami S, Reif B (2013) Proton-detected solid-state NMR at aliphatic sites: applications to crystalline systems. Acc Chem Res 46:2089–2097

Asami S, Schmieder P, Reif B (2010) High resolution 1H-detected solid-state NMR spectroscopy of protein aliphatic resonances: access to tertiary structure information. J Am Chem Soc 132:15133–15135

Austin RH, Chan SS, Jovin TM (1979) Rotational diffusion of cell-surface components by time-resolved phosphoresence anisotropy. Proc Natl Acad Sci USA 76:5650–5654

Bertini I, Luchinat C, Parigi G, Ravera E, Reif B, Turano P (2011) Solid-state NMR of proteins sedimented by ultracentrifugation. Proc Natl Acad Sci USA 108:10396–10399

Bocan J, Pileio G, Levitt MH (2012) Sensitivity enhancement and low-field spin relaxation in singlet NMR. Phys Chem Chem Phys 14:16032–16040

Cady SD, Goodman C, Tatko CD, DeGrado WF, Hong M (2007) Determining the orientation of uniaxially rotating membrane proteins using unoriented samples: a (2)H, (13)C, and (15)N solid-state NMR investigation of the dynamics and orientation of a transmembrane helical bundle. J Am Chem Soc 129:5719–5729

Carulla N, Caddy GL, Hall DR, Zurdo J, Gairi M, Feliz M, Giralt E, Robinson CV, Dobson CM (2005) Molecular recycling within amyloid fibrils. Nature 436:554–558

Chapman MR, Robinson LS, Pinkner JS, Roth R, Heuser J, Hammar M, Normark S, Hultgren SJ (2002) Role of *Escherichia coli* curli operons in directing amyloid fiber formation. Science 295:851–855

Chen K-YM, Zhou F, Fryszczyn BG, Barth P (2012) Naturally evolved G protein-coupled receptors adopt metastable conformations. Proc Natl Acad Sci USA 109:13284–13289

Cherry RJ (1979) Rotational and lateral diffusion of membrane proteins. Biochim Biophys Acta 559:289–327

Cherry RJ (2005) Membrane protein dynamics: rotational dynamics. In: Yeagle PL (ed) The structure of biological membranes. CRC Press, Boca Raton

Chevelkov V, Rehbein K, Diehl A, Reif B (2006) Ultra-high resolution in proton solid-state NMR at high levels of deuteration. Angew Chem Int Ed 45:3878–3881

Chevelkov V, Diehl A, Reif B (2007a) Quantitative measurement of differential ^{15}N-Hα/β T_2 relaxation times in a perdeuterated protein by MAS solid-state NMR spectroscopy. Magn Res Chem 45:S156–S160

Chevelkov V, Faelber K, Schrey A, Rehbein K, Diehl A, Reif B (2007b) Differential line broadening in MAS solid-state NMR due to dynamic interference. J Am Chem Soc 129:10195–10200

Chevelkov V, Zhuravleva AV, Xue Y, Reif B, Skrynnikov NR (2007c) Combined analysis of 15 N relaxation data from solid- and solution-state NMR spectroscopy. J Am Chem Soc 129:12594–12595

Chevelkov V, Diehl A, Reif B (2008) Measurement of ^{15}N–T_1 relaxation rates in a perdeuterated protein by MAS solid-state NMR spectroscopy. J Chem Phys 128:052316

Chevelkov V, Fink U, Reif B (2009a) Accurate determination of order parameters from ^{1}H,^{15}N dipolar couplings in MAS solid-state NMR experiments. J Am Chem Soc 131:14018–14022

Chevelkov V, Fink U, Reif B (2009b) Quantitative analysis of backbone motion in proteins using MAS solid-state NMR spectroscopy. J Biomol NMR 45:197–206

Chevelkov V, Xue Y, Linser R, Skrynnikov NR, Reif B (2010) Comparison of solid-state dipolar couplings and solution relaxation data provides insight into protein backbone dynamics. J Am Chem Soc 132:5015–5017

Cole R, Loria JP (2002) Evidence for flexibility in the function of ribonuclease A. Biochemistry 41:6072–6081

Cowans BA, Grutzner JB (1993) Examination of homogeneous broadening in solids via rotationally synchronized spin-echo NMR-spectroscopy. J Magn Reson, Ser A 105:10–18

Fandrich M, Fletcher MA, Dobson CM (2001) Amyloid fibrils from muscle myoglobin—even an ordinary globular protein can assume a rogue guise if conditions are right. Nature 410:165–166

Fawzi NL, Ying JF, Torchia DA, Clore GM (2010) Kinetics of amyloid beta monomer-to-oligomer exchange by NMR relaxation. J Am Chem Soc 132:9948–9951

Fawzi NL, Ying J, Ghirlando R, Torchia DA, Clore GM (2011) Atomic-resolution dynamics on the surface of amyloid-beta protofibrils probed by solution NMR. Nature 480:268–272

Ferella L, Luchinat C, Ravera E, Rosato A (2013) SedNMR: a web tool for optimizing sedimentation of macromolecular solutes for SSNMR. J Biomol NMR 57:319–326

Fowler DM, Koulov AV, Alory-Jost C, Marks MS, Balch WE, Kelly JW (2006) Functional amyloid formation within mammalian tissue. PLoS Biol 4:100–107

Gardiennet C, Schutz AK, Hunkeler A, Kunert B, Terradot L, Bockmann A, Meier BH (2012) A sedimented sample of a

59 kDa dodecameric helicase yields high-resolution solid-state NMR spectra. Angewandt Chem Int Edtk 51:7855–7858
Garroway AN (1977) Homogeneous and inhomogeneous nuclear spin echoes in organic solids: adamantane. J Magn Reson 28:365–371
Gennis RB (1989) Biomembranes: molecular structure and function. Springer, New York
Good DB, Wang S, Ward ME, Struppe J, Brown LS, Lewandowski JR, Ladizhansky V (2014) Conformational dynamics of a seven transmembrane helical protein anabaena sensory rhodopsin probed by solid-state NMR. J Am Chem Soc 136:2833–2842
Greenwald J, Riek R (2012) On the possible amyloid origin of protein folds. J Mol Biol 421:417–426
Halfmann R, Wright JR, Alberti S, Lindquist S, Rexach M (2012) Prion formation by a yeast GLFG nucleoporin. Prion 6:391–399
Hall DA, Maus DC, Gerfen GJ, Inati SJ, Becerra LR, Dahlquist FW, Griffin RG (1997) Polarization-enhanced NMR spectroscopy of biomolecules in frozen solution. Science 276:930–932
Halle A, Hornung V, Petzold GC, Stewart CR, Monks BG, Reinheckel T, Fitzgerald KA, Latz E, Moore KJ, Golenbock DT (2008) The NALP3 inflammasome is involved in the innate immune response to amyloid-beta. Nat Immunol 9:857–865
Heck M, Hofmann KP (2001) Maximal rate and nucleotide dependence of rhodopsin-catalyzed transducin activation: initial rate analysis based on a double displacement mechanism. J Biol Chem 276:10000–10009
Helmus JJ, Surewicz K, Nadaud PS, Surewicz WK, Jaroniec CP (2008) Molecular conformation and dynamics of the Y145Stop variant of human prion protein in amyloid fibrils. Proc Natl Acad Sci USA 105:6284–6289
Helmus JJ, Surewicz K, Surewicz WK, Jaroniec CP (2010) Conformational flexibility of Y145Stop human prion protein amyloid fibrils probed by solid-state nuclear magnetic resonance spectroscopy. J Am Chem Soc 132:2393–2403
Henzler-Wildman KA, Lei M, Thai V, Kerns SJ, Karplus M, Kern D (2007a) A hierarchy of timescales in protein dynamics is linked to enzyme catalysis. Nature 450:913–916
Henzler-Wildman KA, Thai V, Lei M, Ott M, Wolf-Watz M, Fenn T, Pozharski E, Wilson MA, Petsko GA, Karplus M, Huebner CG, Kern D (2007b) Intrinsic motions along an enzymatic reaction trajectory. Nature 450:838–844
Hiller M, Krabben L, Vinothkumar KR, Castellani F, Van Rossum B, Kühlbrandt W, Oschkinat H (2005) Solid-state magic-angle spinning nmr of outer-membrane protein G from *Escherichia coli*. ChemBioChem 6:1679–1684
Hologne M, Faelber K, Diehl A, Reif B (2005) Characterization of dynamics of perdeuterated proteins by MAS solid-state NMR. J Am Chem Soc 127:11208–11209
Hologne M, Chevelkov V, Reif B (2006) Deuteration of peptides and proteins in MAS solid-state NMR. Prog NMR Spect 48:211–232
Hong M, Doherty T (2006) Orientation determination of membrane-disruptive proteins using powder samples and rotational diffusion: a simple solid-state NMR approach. Chem Phys Lett 432:296–300
Jacso T, Franks WT, Rose H, Fink U, Broecker J, Keller S, Oschkinat H, Reif B (2012) Characterization of membrane proteins in isolated native cellular membranes by dynamic nuclear polarization solid-state NMR spectroscopy without purification and reconstitution. Angew Chem Int Ed 51:432–435
Kato M, Han TNW, Xie S, Shi K, Du X, Wu LC, Mirzaei H, Goldsmith EJ, Longgood J, Pei J, Grishin NV, Frantz DE, Schneider JW, Chen S, Li L, Sawaya MR, Eisenberg D, Tycko R, McKnight SL (2012) Cell-free formation of RNA granules: low complexity sequence domains form dynamic fibers within hydrogels. Cell 149:753–767
Kim HJ, Kim NC, Wang Y-D, Scarborough EA, Moore J, Diaz Z, MacLea KS, Freibaum B, Li S, Molliex A, Kanagaraj AP, Carter R, Boylan KB, Wojtas AM, Rademakers R, Pinkus JL, Greenberg SA, Trojanowski JQ, Traynor BJ, Smith BN, Topp S, Gkazi A-S, Miller J, Shaw CE, Kottlors M, Kirschner J, Pestronk A, Li YR, Ford AF, Gitler AD, Benatar M, King OD, Kimonis VE, Ross ED, Weihl CC, Shorter J, Taylor JP (2013) Mutations in prion-like domains in hnRNPA2B1 and hnRNPA1 cause multisystem proteinopathy and ALS. Nature 495–473: 467
Kitahara R, Hata K, Li H, Williamson MP, Akasaka K (2013) Pressure-induced chemical shifts as probes for conformational fluctuations in proteins. Prog NMR Spect 71:35–58
Klyszejko AL, Shastri S, Mari SA, Grubmuller H, Muller DJ, Glaubitz C (2008) Folding and assembly of proteorhodopsin. J Mol Biol 376:35–41
Knight MJ, Pell AJ, Bertini I, Felli IC, Gonnelli L, Pierattelli R, Herrmann T, Emsley L, Pintacuda G (2012) Structure and backbone dynamics of a microcrystalline metalloprotein by solid-state NMR. Proc Natl Acad Sci USA 109:11095–11100
Krushelnitsky A, Zinkevich T, Reichert D, Chevelkov V, Reif B (2010) Microsecond time scale mobility in a solid protein as studied by the N-15 R-1 rho site-specific NMR relaxation rates. J Am Chem Soc 132:11850–11853
Labokha AA, Gradmann S, Frey S, Hulsmann BB, Urlaub H, Baldus M, Gorlich D (2013) Systematic analysis of barrier-forming FG hydrogels from Xenopus nuclear pore complexes. EMBO J 32:204–218
Lange OF, Lakomek N-A, Fares C, Schroeder GF, Walter KFA, Becker S, Meiler J, Grubmueller H, Griesinger C, de Groot BL (2008) Recognition dynamics up to microseconds revealed from an RDC-derived ubiquitin ensemble in solution. Science 320:1471–1475
Le YY, Gong WH, Tiffany HL, Tumanov A, Nedospasov S, Shen WP, Dunlop NM, Gao JL, Murphy PM, Oppenheim JJ, Wang JM (2001) Amyloid beta(42) activates a G-protein-coupled chemoattractant receptor, FPR-Like-1. J Neurosci 21:RC123
Lewandowski JR, Dumez JN, Akbey U, Lange S, Emsley L, Oschkinat H (2011a) Enhanced resolution and coherence lifetimes in the solid-state NMR spectroscopy of perdeuterated proteins under ultrafast magic-angle spinning. J Phys Chem Lett 2:2205–2211
Lewandowski JR, Sass HJ, Grzesiek S, Blackledge M, Emsley L (2011b) Site-specific measurement of slow motions in proteins. J Am Chem Soc 133:16762–16765
Linser R, Chevelkov V, Diehl A, Reif B (2007) Sensitivity enhancement using paramagnetic relaxation in MAS solid state NMR of perdeuterated proteins. J Magn Reson 189:209–216
Linser R, Fink U, Reif B (2010) Detection of dynamic regions in biological solids enabled by spin-state selective NMR experiments. J Am Chem Soc 132:8891–8893
Linser R, Dasari M, Hiller M, Higman V, Fink U, Lopez del Amo J-M, Handel L, Kessler B, Schmieder P, Oesterhelt D, Oschkinat H, Reif B (2011) Proton detected solid-state NMR of fibrillar and membrane proteins. Angew Chem Int Ed 50:4508–4512
Lopez del Amo J-M, Dasari M, Fink U, Grelle G, Wanker EE, Bieschke J, Reif B (2012a) Structural properties of EGCG induced, non-toxic Alzheimer's disease Aβ oligomers. J Mol Biol 421:517–524
Lopez del Amo JM, Schmidt M, Fink U, Dasari M, Fändrich M, Reif B (2012b) The basic subunit in Alzheimer's disease beta-amyloid fibrils can be an asymmetric dimer. Angew Chem Int Ed 51:6136–6139
Lopez del Amo J-M, Schneider D, Loquet A, Lange A, Reif B (2013) Cryogenic solid state NMR studies of fibrils of the Alzheimer's disease amyloid-β peptide: perspectives for DNP. J Biomol NMR 56:359–363
Lu GJ, Park SH, Opella SJ (2012) Improved H-1 amide resonance line narrowing in oriented sample solid-state NMR of membrane proteins in phospholipid bilayers. J Magn Reson 220:54–61

Luecke H, Schobert B, Richter HT, Cartailler JP, Lanyi JK (1999) Structure of bacteriorhodopsin at 1.55 angstrom resolution. J Mol Biol 291:899–911

Maddelein ML, Dos Reis S, Duvezin-Caubet S, Coulary-Salin B, Saupe SJ (2002) Amyloid aggregates of the HET-s prion protein are infectious. Proc Natl Acad Sci USA 99:7402–7407

Mainz A, Jehle S, van Rossum BJ, Oschkinat H, Reif B (2009) Large protein complexes with extreme rotational correlation times investigated in solution by magic-angle-spinning NMR spectroscopy. J Am Chem Soc 131:15968–15969

Mainz A, Bardiaux B, Kuppler F, Multhaup G, Felli IC, Pierattelli R, Reif B (2012) Structural and mechanistic implications of metal-binding in the small heat-shock protein αB-crystallin. J Biol Chem 287:1128–1138

Mainz A, Religa T, Sprangers R, Linser R, Kay LE, Reif B (2013) NMR spectroscopy of soluble protein complexes at one megadalton and beyond. Angewandt Chem Int Edt 52:8746–8751

Maji SK, Perrin MH, Sawaya MR, Jessberger S, Vadodaria K, Rissman RA, Singru PS, Nilsson KPR, Simon R, Schubert D, Eisenberg D, Rivier J, Sawchenko P, Vale W, Riek R (2009) Functional amyloids as natural storage of peptide hormones in pituitary secretory granules. Science 325:328–332

Mollica L, Baias M, Lewandowski JR, Wylie BJ, Sperling LJ, Rienstra CM, Emsley L, Blackledge M (2012) Atomic-resolution structural dynamics in crystalline proteins from NMR and molecular simulation. J Phys Chem Lett 3:3657–3662

Morris VK, Linser R, Wilde KL, Duff AP, Sunde M, Kwan AH (2012) Solid-state NMR spectroscopy of functional amyloid from a fungal hydrophobin: a well-ordered beta-sheet core amidst structural heterogeneity. Angewandt Chem Int Edt 51:12621–12625

Narayanan S, Reif B (2005) Characterization of chemical exchange between soluble and aggregated states of beta-amyloid by solution state NMR upon variation of the salt conditions. Biochemistry 44:1444–1452

Paravastu AK, Leapman RD, Yau W-M, Tycko R (2008) Molecular structural basis for polymorphism in Alzheimer's beta-amyloid fibrils. Proc Natl Acad Sci USA 105:18349–18354

Park SH, Mrse AA, Nevzorov AA, De Angelis AA, Opella SJ (2006) Rotational diffusion of membrane proteins in aligned phospholipid bilayers by solid-state NMR spectroscopy. J Magn Reson 178:162–165

Park SH, Das BB, Casagrande F, Tian Y, Nothnagel HJ, Chu M, Kiefer H, Maier K, De Angelis AA, Marassi FM, Opella SJ (2012) Structure of the chemokine receptor CXCR1 in phospholipid bilayers. Nature 491:779

Patzelt H, Ulrich AS, Egbringhoff H, Dux P, Ashurst J, Simon B, Oschkinat H, Oesterhelt D (1997) Towards structural investigations on isotope labelled native bacteriorhodopsin in detergent micelles by solution-state NMR spectroscopy. J Biomol NMR 10:95–106

Petkova AT, Yau W-M, Tycko R (2006) Experimental constraints on quaternary structure in Alzheimer's β-amyloid fibrils. Biochemistry 45:498–512

Qiang W, Kelley K, Tycko R (2013) Polymorph-specific kinetics and thermodynamics of beta-amyloid fibril growth. J Am Chem Soc 135:6860–6871

Quillin ML, Matthews BW (2000) Accurate calculation of the density of proteins. Acta Crystallogr Sect D: Biol Crystallogr 56:791–794

Rasmussen SGF, Choi H-J, Rosenbaum DM, Kobilka TS, Thian FS, Edwards PC, Burghammer M, Ratnala VRP, Sanishvili R, Fischetti RF, Schertler GFX, Weis WI, Kobilka BK (2007) Crystal structure of the human ß2 adrenergic G-protein-coupled receptor. Nature 450:383–388

Ravera E, Parigi G, Mainz A, Religa TL, Reif B, Luchinat C (2013) Experimental determination of microsecond reorientation correlation times in protein solutions. J Phys Chem B 117:3548–3553

Renault M, Pawsey S, Bos MP, Koers EJ, Nand D, Tommassen-van Boxtel R, Rosay M, Tommassen J, Maas WE, Baldus M (2011) Solid-state NMR spectroscopy on cellular preparations Enhanced by dynamic nuclear polarization. Angew Chem Int Ed Engl 51:2998–3001

Rose A, Theune D, Goede A, Hildebrand PW (2013) MP:PD—a data base of internal packing densities, internal packing defects and internal waters of helical membrane proteins. Nucl Acids Res (in press)

Rosenbaum DM, Cherezov V, Hanson MA, Rasmussen SGF, Thian FS, Kobilka TS, Choi H-J, Yao X-J, Weis WI, Stevens RC, Kobilka BK (2007) GPCR engineering yields high-resolution structural insights into ß2-adrenergic receptor function. Science 318:1266–1273

Saffman PG, Delbruck M (1975) Brownian motion in biological membranes. Proc Natl Acad Sci USA 72:3111–3113

Samoson A, Tuherm T, Gan Z (2001) High-field high-speed mas resolution enhancement in 1H NMR spectroscopy of solids. Solid State NMR 20:130–136

Sapra KT, Besir S, Oesterhelt D, Muller DJ (2006) Characterizing molecular interactions in different bacteriorhodopsin assemblies by single-molecule force spectroscopy. J Mol Biol 355:640–650

Sarkar CA, Dodevski I, Kenig M, Dudli S, Mohr A, Hermans E, Plückthun A (2008) Directed evolution of a G protein-coupled receptor for expression, stability, and binding selectivity. Proc Natl Acad Sci USA 105:14808–14813

Schanda P, Meier BH, Ernst M (2010) Quantitative analysis of protein backbone dynamics in microcrystalline ubiquitin by solid-state NMR spectroscopy. J Am Chem Soc 132:15957–15967

Schanda P, Huber M, Boisbouvier J, Meier BH, Ernst M (2011) Solid-state NMR measurements of asymmetric dipolar couplings provide insight into protein side-chain motion. Angewandt Chem Int Edt 50:11005–11009

Schlinkmann KM, Honegger A, Tureci E, Robison KE, Lipovsek D, Pluckthun A (2012) Critical features for biosynthesis, stability, and functionality of a G protein-coupled receptor uncovered by all-versus-all mutations. Proc Natl Acad Sci USA 109:9810–9815

Shahid SA, Bardiaux B, Franks WT, Krabben L, Habeck M, van Rossum B-J, Linke D (2012) Membrane-protein structure determination by solid-state NMR spectroscopy of microcrystals. Nat Methods 9:U1119–U1212

Skrynnikov NR (2007) Asymmetric doublets in MAS NMR: coherent and incoherent mechanisms. Magn Res Chem 45:S161–S173

Soscia SJ, Kirby JE, Washicosky KJ, Tucker SM, Ingelsson M, Hyman B, Burton MA, Goldstein LE, Duong S, Tanzi RE, Moir RD (2010) The Alzheimer's disease-associated amyloid beta-protein is an antimicrobial peptide. PloS One 5:e9505

Stein WD (1990) Channels, carriers and pumps. An introduction to membrane transport. Academic Press, San Diego

Takahashi H, Ayala I, Bardet M, De Paepe G, Simorre J-P, Hediger S (2013) Solid-state NMR on bacterial cells: selective cell wall signal enhancement and resolution improvement using dynamic nuclear polarization. J Am Chem Soc 135:5105–5110

Tanzi RE, Moir RD, Wagner SL (2004) Clearance of Alzheimer's A beta peptide: the many roads to perdition. Neuron 43:605–608

Tollinger M, Sivertsen AC, Meier BH, Ernst M, Schanda P (2012) Site-resolved measurement of microsecond-to-millisecond conformational-exchange processes in proteins by solid-state NMR spectroscopy. J Am Chem Soc 134:14800–14807

Tycko R (2006) Molecular structure of amyloid fibrils: insights from solid-state NMR. Quart Rev Biophys 39:1–55

Ueno H, Suzuki T, Kinosita KJ, Yoshida M (2005) ATP-driven stepwise rotation of FoF1-ATP synthase. Proc Natl Acad Sci USA 102:1333–1338

Vanderhart DL, Earl WL, Garroway AN (1981) Resolution in C-13 NMR of organic-solids using high-power proton decoupling and magic-angle sample spinning. J Magn Reson 44:361–401

Wang S, Munro RA, Shi L, Kawamura I, Okitsu T, Wada A, Kim S-Y, Jung K-H, Brown LS, Ladizhansky V (2013a) Solid-state NMR spectroscopy structure determination of a lipid-embedded heptahelical membrane protein. Nat Methods 10:1007

Wang T, Park YB, Caporini MA, Rosay M, Zhong L, Cosgrove DJ, Hong M (2013b) Sensitivity-enhanced solid-state NMR detection of expansin's target in plant cell walls. Proc Natl Acad Sci USA 110:16444–16449

Ward ME, Shi L, Lake E, Krishnamurthy S, Hutchins H, Brown LS, Ladizhansky V (2011) Proton-detected solid-state NMR reveals intramembrane polar networks in a seven-helical transmembrane protein proteorhodopsin. J Am Chem Soc 133:17434–17443

Wasmer C, Lange A, Van Melckebeke H, Siemer AB, Riek R, Meier BH (2008) Amyloid fibrils of the HET-s(218-289) prion form a beta solenoid with a triangular hydrophobic core. Science 319:1523–1526

Wiench JW, Lin VS-Y, Pruski M (2008) Si-29 NMR in solid state with CPMG acquisition under MAS. J Magn Reson 193:233–242

Williams JC, McDermott AE (1995) Dynamics of the flexible loop of triosephosphate isomerase—the loop motion is not ligand-gated. Biochemistry 34:8309–8319

Yang J, Tasayco ML, Polenova T (2009) Dynamics of reassembled thioredoxin studied by magic angle spinning NMR: snapshots from Different Time Scales. J Am Chem Soc 131:13690–13702

Zhou DH, Shah G, Cormos M, Mullen C, Sandoz D, Rienstra CM (2007a) Proton-detected solid-state NMR Spectroscopy of fully protonated proteins at 40 kHz magic-angle spinning. J Am Chem Soc 129:11791–11801

Zhou DH, Shea JJ, Nieuwkoop AJ, Franks WT, Wylie BJ, Mullen C, Sandoz D, Rienstra CM (2007b) Solid-state protein-structure determination with proton-detected triple-resonance 3D magic-angle-spinning NMR spectroscopy. Angew Chemie Int Edt 46:8380–8383

Zhou DH, Nieuwkoop AJ, Berthold DA, Comellas G, Sperling LJ, Tang M, Shah GJ, Brea EJ, Lemkau LR, Rienstra CM (2012) Solid-state NMR analysis of membrane proteins and protein aggregates by proton detected spectroscopy. J Biomol NMR 54:291–305

Zinkevich T, Chevelkov V, Reif B, Saalwachter K, Krushelnitsky A (2013) Internal protein dynamics on ps to μs timescales as studied by multi-frequency 15 N solid-state NMR relaxation. J Biomol NMR 57:219–235